

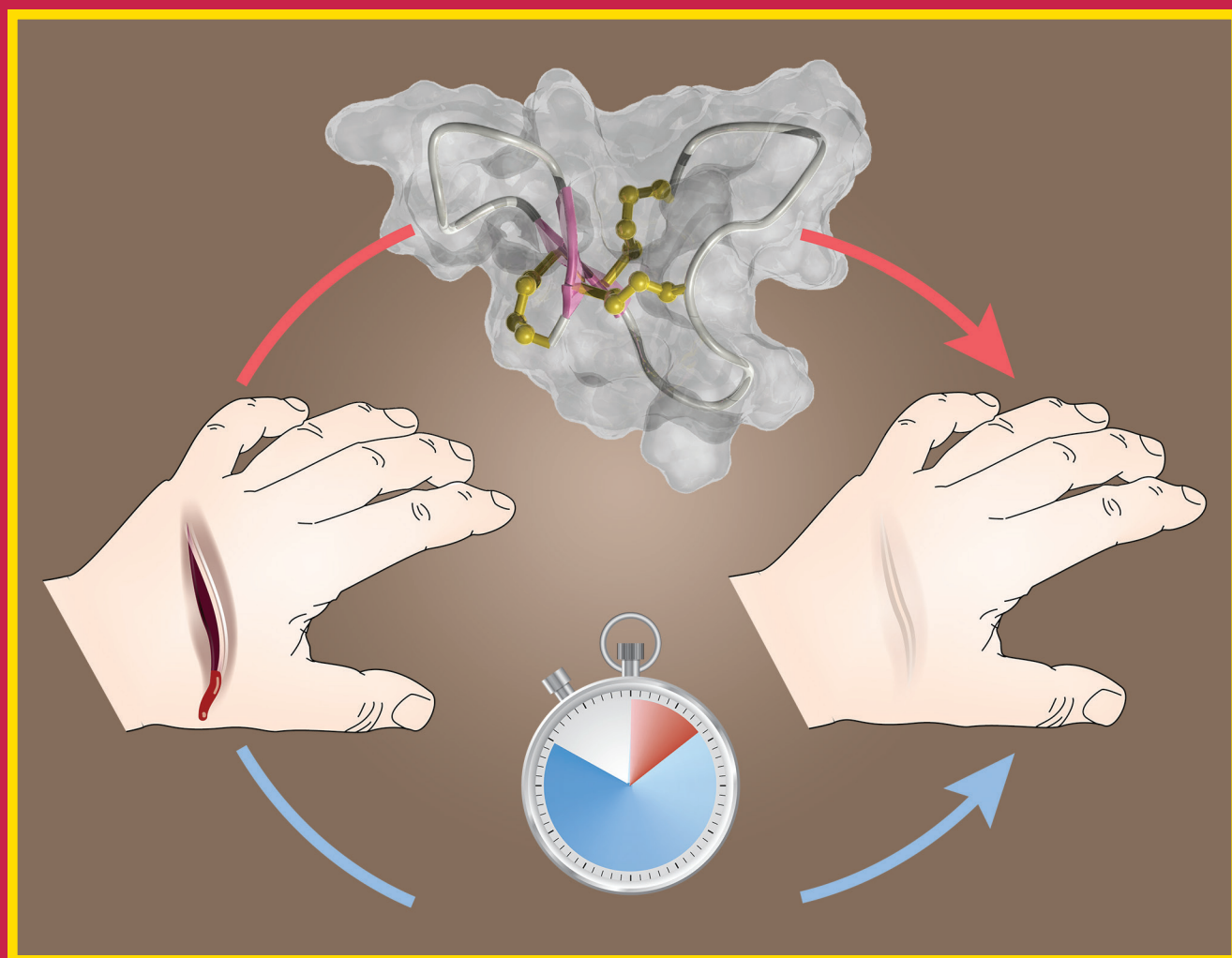
May 25, 2017

Volume 60 • Number 10

[pubs.acs.org/jmc](http://pubs.acs.org/jmc)

CELEBRATING **60<sup>th</sup>** VOLUME

# Journal of Medicinal Chemistry



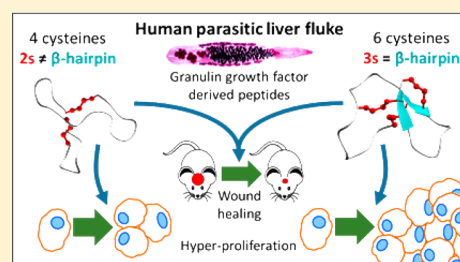


## Development of a Potent Wound Healing Agent Based on the Liver Fluke Granulin Structural Fold

Paramjit S. Bansal,<sup>†,§</sup> Michael J. Smout,<sup>†,§</sup> David Wilson,<sup>†</sup> Claudia Cobos Caceres,<sup>†</sup> Mohadeseh Dastpeyman,<sup>†</sup> Javier Sotillo,<sup>†</sup> Julia Seifert,<sup>†</sup> Paul J. Brindley,<sup>‡</sup> Alex Loukas,<sup>\*,†</sup> and Norelle L. Daly<sup>\*,†</sup><sup>†</sup>Centre for Biodiscovery and Molecular Development of Therapeutics, Australian Institute of Tropical Health and Medicine, James Cook University, Cairns 4870, Queensland Australia<sup>‡</sup>Department of Microbiology, Immunology and Tropical Medicine and Research Center for Neglected Diseases of Poverty, School of Medicine and Health Sciences, George Washington University, Washington D.C. 20037, United States

## S Supporting Information

**ABSTRACT:** Granulins are a family of protein growth factors that are involved in cell proliferation. An orthologue of granulin from the human parasitic liver fluke *Opisthorchis viverrini*, known as *Ov*-GRN-1, induces angiogenesis and accelerates wound repair. Recombinant *Ov*-GRN-1 production is complex and poses an obstacle for clinical development. To identify the bioactive region(s) of *Ov*-GRN-1, four truncated N-terminal analogues were synthesized and characterized structurally using NMR spectroscopy. Peptides that contained only two native disulfide bonds lack the characteristic granulin  $\beta$ -hairpin structure. Remarkably, the introduction of a non-native disulfide bond was critical for formation of  $\beta$ -hairpin structure. Despite this structural difference, both two and three disulfide-bonded peptides drove proliferation of a human cholangiocyte cell line and demonstrated potent wound healing in mice. Peptides derived from *Ov*-GRN-1 are leads for novel wound healing therapeutics, as they are likely less immunogenic than the full-length protein and more convenient to produce.



## INTRODUCTION

Granulins are a family of protein growth factors involved in a wide range of physiological functions and disease processes including embryogenesis, wound repair, inflammation, and tumor growth.<sup>1</sup> The human parasitic liver fluke *Opisthorchis viverrini* secretes a granulin family member called *Ov*-GRN-1, which was originally isolated from the excretory/secretory (ES) products of the carcinogenic trematode.<sup>2,3</sup> *Ov*-GRN-1 was the first growth factor described from a pathogen to cause proliferation of both human and murine cells.<sup>4,5</sup> We have shown that picomoles of recombinant *Ov*-GRN-1 induce angiogenesis and accelerate wound repair in mice upon topical administration, findings that indicate that liver fluke granulin might be developed as a treatment for wounds.<sup>6</sup>

An understanding of the structure–activity relationship for *Ov*-GRN-1 would enable design of the most efficacious form of this granulin for healing wounds. The three-dimensional structure of *Ov*-GRN-1 has not been experimentally determined, but structures for granulins of several species have been reported. The initial granulin structure determined was that of carp granulin-1; this comprises four  $\beta$ -hairpins cross-linked together by six disulfide bonds in a ladder-shaped arrangement of the disulfide bonds.<sup>7</sup> Despite the well-defined structure observed for carp granulin-1, the structure function relationships of granulins are complex and appear to be highly dependent on the primary sequence. This is particularly evident

with the human granulins. The precursor protein of mammalian granulin (progranulin, PGRN) contains seven-and-a-half granulin domains that are approximately 6 kDa in molecular mass and are proteolytically processed into individual granulin modules after secretion of PGRN from the cell.<sup>1</sup> The “half-granulin” unit, termed paraganulin, contains only six cysteine residues.<sup>8</sup>

The seven human granulin modules have been expressed individually and the structures analyzed by NMR spectroscopy.<sup>9</sup> Three contain relatively well-defined three-dimensional structures in solution (A, C, and F), whereas the others are mainly mixtures of poorly structured disulfide isomers.<sup>9</sup> The structure of human granulin A includes a  $\beta$ -hairpin structure similar to carp granulin-1, but there is significant structural disorder in the C-terminal region. Of the well-folded human granulin modules, granulin A demonstrates potent inhibition of proliferation of a breast cancer cell line, while by contrast, human granulin F stimulates cell proliferation.<sup>9</sup> The poorly folded peptides exhibit weak or no inhibitory or activity. It should be noted, however, that the limited activity may be due to the absence of key signaling pathways in the target cells, and/or that the production of the recombinant peptides in bacteria induced incomplete/incorrect folding. To date, the

Received: February 2, 2017

Published: April 20, 2017

range of granulin activities and binding partners is broad and seemingly organ- and cofactor-dependent.<sup>10–13</sup>

Structural analysis with NMR spectroscopy has shown that the N-terminal regions of carp granulin-1 and human granulin A can fold independently of the C-terminal regions.<sup>14,15</sup> Truncated analogues of these two granulins containing only two-disulfide bonds have  $\beta$ -hairpin structures, as shown for a 30-residue N-terminal domain of carp granulin-1 (Figure 1). In

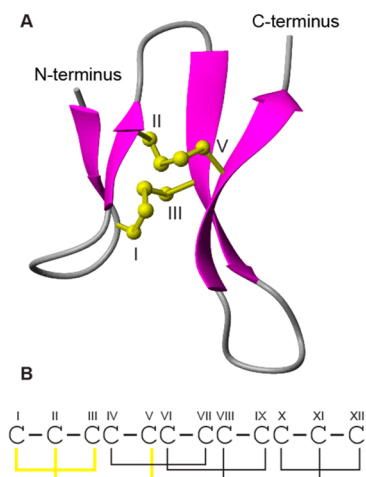


**Figure 1.** Three-dimensional structure of a 30 residue N-terminal domain of carp granulin-1. (A) PDB code 1QGM, the  $\beta$ -strands are shown as purple arrows and the disulfide bonds in yellow ball and stick format. The image was generated using MOLMOL. (B) The disulfide connectivity in the full length carp granulin-1 protein.<sup>7</sup> Cysteines are designated with sequential roman numerals I–XII. The two bonds in the truncated carp granulin-1 are highlighted in yellow.

the current study, we synthesized truncated versions of *Ov*-GRN-1 to determine if this region can fold independently and to determine if the N-terminal region contributes to cell proliferation and wound healing. We show for the first time that the N-terminal region of *Ov*-GRN-1 displays novel folding properties, and notably, from a drug design perspective, peptides derived from the N-terminus are as potent as the full-length protein and Regranex, a clinically used wound-healing agent, in healing cutaneous wounds in laboratory mice.

## RESULTS

**Design and Synthesis of Truncated *Ov*-GRN-1 Peptides.** To determine if the N-terminal region of *Ov*-GRN-1 can fold independently, several truncated peptides were designed and synthesized using Fmoc chemistry. The sequences of the synthetic peptides are shown in Figure 2A.

*Ov*-GRN<sub>1–35</sub>, *Ov*-GRN<sub>8–38</sub>, and *Ov*-GRN<sub>12–34</sub> all contain four cysteine residues equivalent to Cys I, Cys II, Cys III, and Cys V in the full-length protein (for the remainder of the report, Roman numerals refer to the numbering present in the full length protein). Cys IV and Cys VI were predicted to form disulfide bonds with Cys VII and Cys IX, respectively, based on the three-dimensional structure of carp granulin-1.<sup>7</sup> In the truncated analogues, Cys IV and Cys VI were replaced with alanine residues to prevent disulfide bond formation between these residues. Selective protection of the cysteine residues was used to direct the folding to form the predicted disulfide connectivity (i.e., Cys I–Cys III and Cys II–Cys V).

*Ov*-GRN-1 contains an extended N-terminal tail (11 residues prior to the first cysteine residue) not present in the majority of granulins, and these residues were included in *Ov*-GRN<sub>1–35</sub> to determine if they play a role in the bioactivity. The N-terminus was truncated and the C-terminus extended in *Ov*-GRN<sub>8–38</sub> to provide an analogue with a similar number of residues to the carp granulin-1 truncated peptide. *Ov*-GRN<sub>12–34</sub> is the minimal sequence that contains the four cysteine residues (CysI, CysII, CysIII, and CysV) and was designed to determine if the N- and C-terminal regions are required for folding and activity.

An additional peptide was synthesized (*Ov*-GRN<sub>12–35\_3s</sub>) with a truncated N-terminus but containing the first six cysteines of *Ov*-GRN-1 (the “3s” refers to the presence of three-disulfide bonds in the peptide). This peptide is analogous to mammalian paragrulin (above) in terms of the cysteine residues. It was synthesized without selective protection of the cysteine residues, and the major conformation was purified for analysis of its structure and activity.

**Structural Analysis with NMR Spectroscopy.** NMR spectroscopy was employed to analyze the structure of the peptides. The one-dimensional spectra of *Ov*-GRN<sub>1–35</sub>, *Ov*-GRN<sub>8–38</sub>, and *Ov*-GRN<sub>12–34</sub> have limited dispersion in the amide regions consistent with a lack of  $\beta$ -sheet structures despite formation of the two native disulfide bonds. Two-dimensional spectra (TOCSY and NOESY) were used to assign the resonances, and the secondary shifts were determined by subtracting random coil shifts<sup>16</sup> from the  $\alpha$ H shifts. The secondary shifts are similar over the equivalent residues for these three peptides, as shown in Figure 2B, indicating that the structures were similar and, consequently, that the differences in the N- and C-termini of these peptides did not influence the overall fold. Furthermore, the secondary shifts were consistent with a lack of  $\beta$ -sheet structure as they are primarily negative and  $\beta$ -sheet structures are characterized by positive secondary shifts. The three-dimensional structure of *Ov*-GRN<sub>12–34</sub> was determined using NMR spectroscopy, as shown in Figure 3. In contrast to the characteristic granulin fold, the structure comprised turns and a region of  $3_{10}$  helix. The structure statistics are provided in Supporting Information, Table S1.

In contrast to the two-disulfide bond-containing *Ov*-GRN-1 peptides, *Ov*-GRN<sub>12–35\_3s</sub> with three-disulfide bonds, has more dispersion in the amide region in the one-dimensional NMR spectrum. Furthermore, additional peaks were present in the spectra, likely due to isomerization of the proline residues. Despite these additional peaks, the major conformation was fully assigned and the secondary shifts were similar to the truncated carp granulin-1<sup>14</sup> (Figure 3), which indicates the similarity of the overall structures. Truncated carp granulin-1, comprising residues 1–30, has previously been synthesized with Cys IV and Cys VI replaced with serine residues and was shown to form a  $\beta$ -sheet structure.<sup>14</sup> Here we synthesized carp granulin<sub>1–30</sub> with Cys IV and Cys VI replaced with alanine residues to be consistent with the truncated peptides of *Ov*-GRN-1. Only minor variations were evident between the published<sup>14</sup> chemical shifts of carp granulin-1 with the serine substitutions and the peptide with the alanine substitutions (Supporting Information, Figure S1), indicating that the overall fold is still maintained.

To confirm if the structure of *Ov*-GRN<sub>12–35\_3s</sub> was similar to carp granulin<sub>1–30</sub>, three-dimensional structures were calculated using CYANA. Structures were initially calculated without disulfide bond restraints. In these structures, a  $\beta$ -hairpin was present from residues 14–23, but residues 1–8 were not

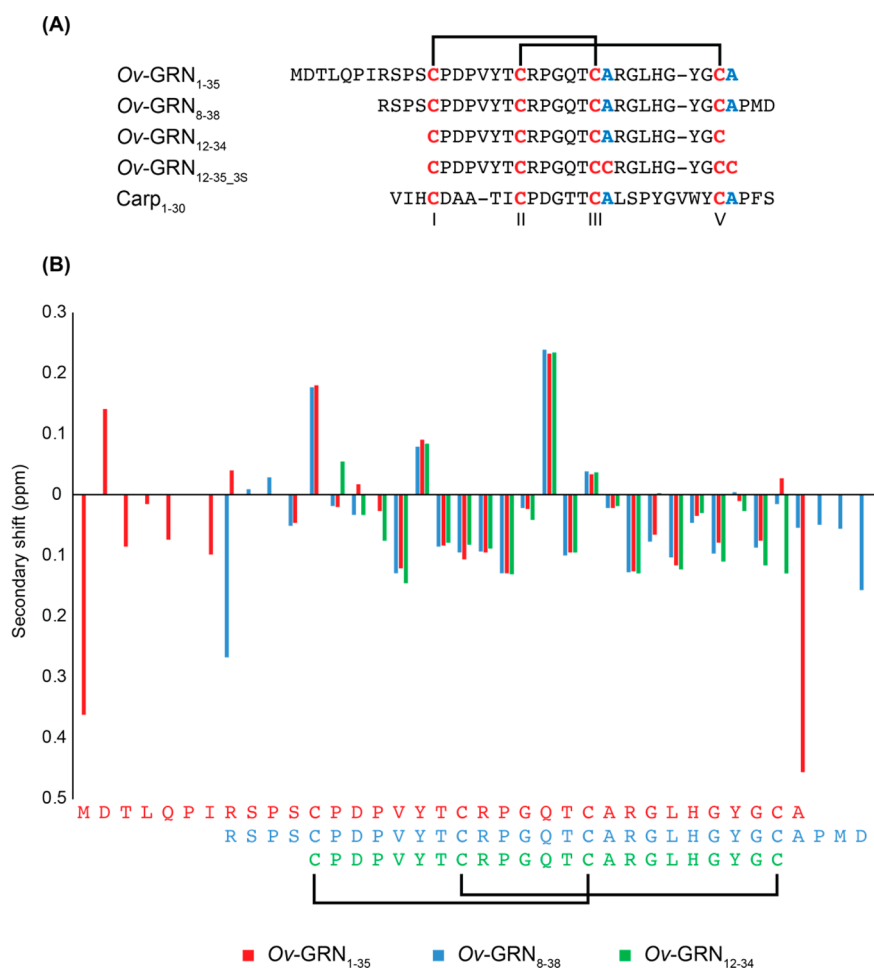


**Figure 2.** Sequences and secondary shifts of the *Ov*-GRN-1 truncated analogues. (A) Sequences show Cys IV and Cys VI were replaced with alanine residues; the cysteines are highlighted in red, and the substitutions are shown in blue. The N-terminal 30 residues of carp granulin-1 is also provided, with Cys IV and Cys VI replaced with alanine residues. (B) Secondary shifts of *Ov*-GRN-1 peptides with four cysteine residues (*Ov*-GRN<sub>1–35</sub>, *Ov*-GRN<sub>8–38</sub>, and *Ov*-GRN<sub>12–34</sub>). The secondary shifts were derived by subtracting random coil shifts<sup>16</sup> from the  $\alpha$ H shifts. The similarity in the secondary shifts for the conserved residues indicates that the overall fold is the same in the three peptides. Color scheme is retained in Figures 2–5. Both panels: black connecting lines represent disulfide bond connectivity.

defined. The lack of definition for residues 1–8 prevented an analysis of the sulfur–sulfur distances, providing insight into the most likely connectivity. Therefore, an alternative approach was used whereby the structures were calculated with the 15 possible disulfide bond connectivities. This approach has previously been used for disulfide-rich peptides such as the cyclotides to analyze the disulfide bond connectivities.<sup>17,18</sup> The CYANA target functions for the 15 connectivities for *Ov*-GRN<sub>12–35\_3s</sub> are shown in Supporting Information, Table S2. The connectivity with the lowest CYANA target function was Cys I–Cys III, Cys II–Cys V, and Cys IV–Cys VI. The three-dimensional structure of *Ov*-GRN<sub>12–35\_3s</sub> with this connectivity is shown in Figure 3 and the structure statistics provided in Supporting Information, Table S1. The most well-defined region of the molecule was the  $\beta$ -hairpin between residues 14–23. The N-terminal region, encompassing Cys I and Cys II, displayed marked structural disorder.

**Cell Proliferation.** The influence of the *Ov*-GRN-1 peptides on proliferation of H69 cholangiocytes in real time was assessed using xCELLigence technology, and dose response curves were determined for the peptides. *Ov*-GRN<sub>12–35\_3s</sub> at a final concentration of 2  $\mu$ M, resulted in a 41% increase in cell growth compared to control peptide ( $p < 0.0001$ ) (Figure 4A).

A dose response curve similar to that obtained for *Ov*-GRN-1 was observed with *Ov*-GRN<sub>12–35\_3s</sub> treatment, characterized by significantly increased cell proliferation at final concentrations of  $\geq 15$  nM ( $p < 0.05$ ). The two-disulfide bonded *Ov*-GRN-1 peptides were less potent at nanomolar concentrations but at 2  $\mu$ M promoted significant cell proliferation (14–25% above peptide control;  $p < 0.01$ ) with dose response curves typified by *Ov*-GRN<sub>12–34</sub> (Figure 4A). No cell cytotoxicity was observed for any of the peptides tested at concentrations up to 2  $\mu$ M.

The cell proliferation observed for the *Ov*-GRN peptides is in contrast to carp granulin<sub>1–30</sub> that induced minimal cell proliferation (nonsignificant) at all concentrations tested and maximum proliferation of 9% over peptide controls at 32 nM. The response at 400 nM of all the *Ov*-GRN peptides (Figure 4B) highlights the enhanced potency of the three-disulfide bonded peptide (*Ov*-GRN<sub>12–35\_3s</sub>) compared to the two-disulfide bonded peptides. *Ov*-GRN<sub>12–35\_3s</sub> promoted a highly significant ( $p < 0.0001$ ) increase in cell proliferation (26% over peptide controls) compared to the remaining peptides that induced minimal proliferation, of which the most potent was *Ov*-GRN<sub>1–35</sub> (9% nonsignificant increase over peptide control).

**Mouse Wound Healing Model.** The truncated *Ov*-GRN-1 peptides formulated with methylcellulose were tested in a

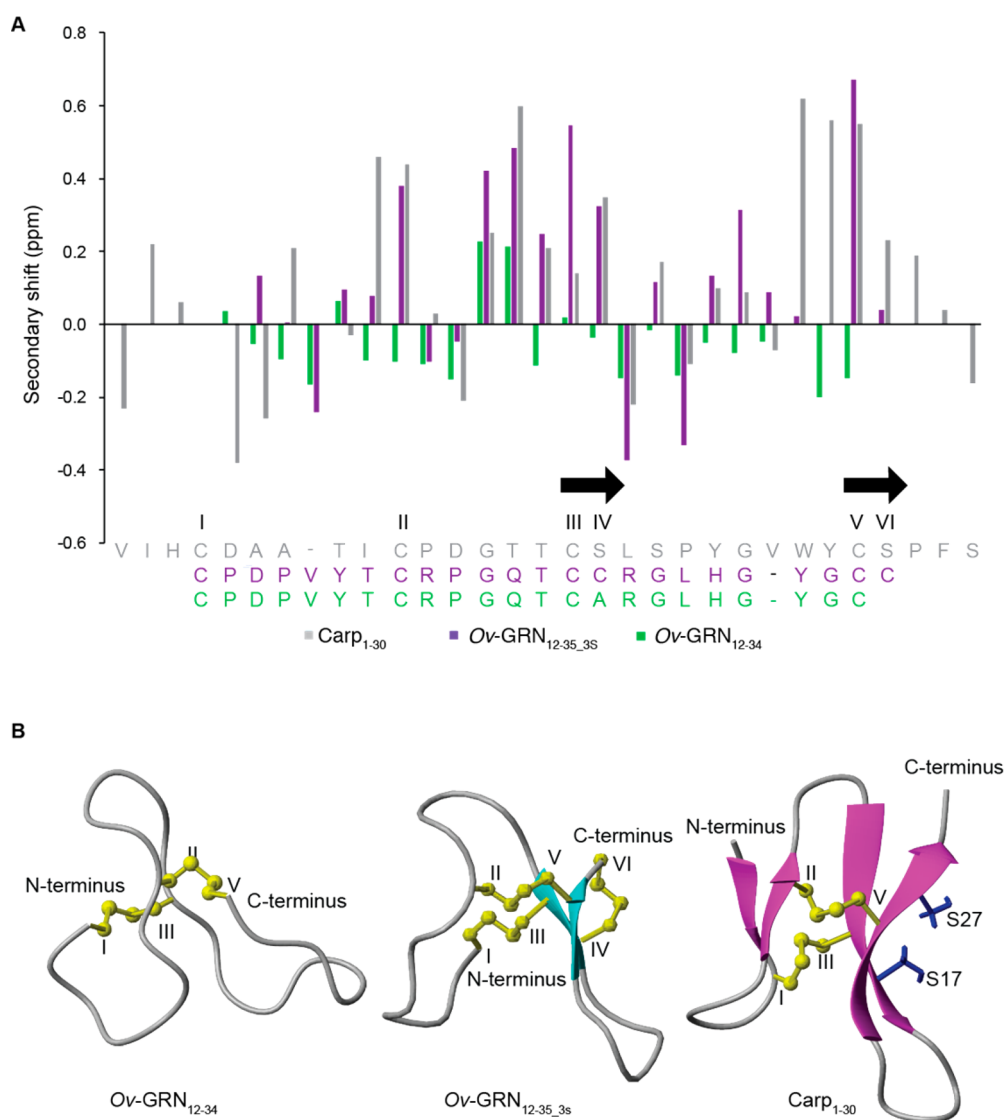


**Figure 3.** Structural analysis of *Ov-GRN*<sub>12-34</sub> and *Ov-GRN*<sub>12-35\_3s</sub>. (A) Secondary shifts of *Ov-GRN*<sub>12-34</sub> and *Ov-GRN*<sub>12-35\_3s</sub> compared to carp granulin<sub>1-30</sub>. The secondary shifts were derived by subtracting random coil shifts<sup>16</sup> from the  $\alpha$ H shifts. *Ov-GRN*<sub>12-34</sub> has significantly different secondary shifts compared to *Ov-GRN*<sub>12-35\_3s</sub> and carp<sub>1-30</sub> and lacks positive shifts, indicating a lack of  $\beta$ -sheet structure. Despite the differences in sequence, the trends for the secondary shifts between *Ov-GRN*<sub>12-35\_3s</sub> and carp<sub>1-30</sub> are similar, indicating that the  $\beta$ -sheet present in carp granulin-1 is also present in *Ov-GRN*<sub>12-35\_3s</sub> (black arrows). (B) The structures of *Ov-GRN*<sub>12-34</sub> and *Ov-GRN*<sub>12-35\_3s</sub> were determined using NMR spectroscopy and confirms that *Ov-GRN*<sub>12-34</sub> does not contain  $\beta$ -sheet structure but *Ov-GRN*<sub>12-35\_3s</sub> does (blue arrows). Disulfide bonds are shown as yellow ball and stick representations, and the structure of carp<sub>1-30</sub> are shown for comparison. The side chains of residues Ser17 and Ser27 are highlighted on the carp<sub>1-30</sub> structure to indicate the Cys–Ser substituted sites of Cys IV and Cys VI. On the basis of this structure, it appears likely that Cys IV and Cys VI of carp<sub>1-30</sub> could form a disulfide bond, consistent with the likely connectivity in *Ov-GRN*<sub>12-35\_3s</sub>.

mouse model of wound healing. All *Ov-GRN*-1 peptides exhibited potent activity (Figure 5A,B) when applied topically compared to control peptide in methylcellulose. The *Ov-GRN*-1 peptides, *Ov-GRN*-1 protein, and Regranex significantly improved healing compared to peptide control on days 2–4 ( $p < 0.05$ ). As wounds closed, differences among treatments waned and significant differences were unapparent beyond day 4. Regranex and the various granulin peptides showed near identical best-fit curves, and intact *Ov-GRN*-1 was the only compound tested here that provided significant improvement over Regranex on days 3 and 4 ( $p < 0.05$ ; Figure 5B). Significant differences were not observed between the various negative control groups formulated with methylcellulose, including PBS vehicle control, peptide control, and thioredoxin (TRX) recombinant protein control.

When healing at day 4 (Figure 5C, Supporting Information, Figure S2) was evaluated relative to PBS vehicle from each biological replicate, treatment of wounds with *Ov-GRN*-1 protein and peptides significantly accelerated wound healing compared to controls ( $p < 0.01$  at day 4:26–41% over PBS). Although the *Ov-GRN*-1 protein, *Ov-GRN*<sub>1-35</sub>, and *Ov-GRN*<sub>12-34</sub> (37–41% over PBS) provided improved healing compared to Regranex (29% over PBS), none of these comparisons reached significance at the day 4 time point.

## DISCUSSION

Elucidating the structure/activity relationships of granulins has been challenging given the sequence and structural variations in this protein family. Regions with bioactivity are poorly

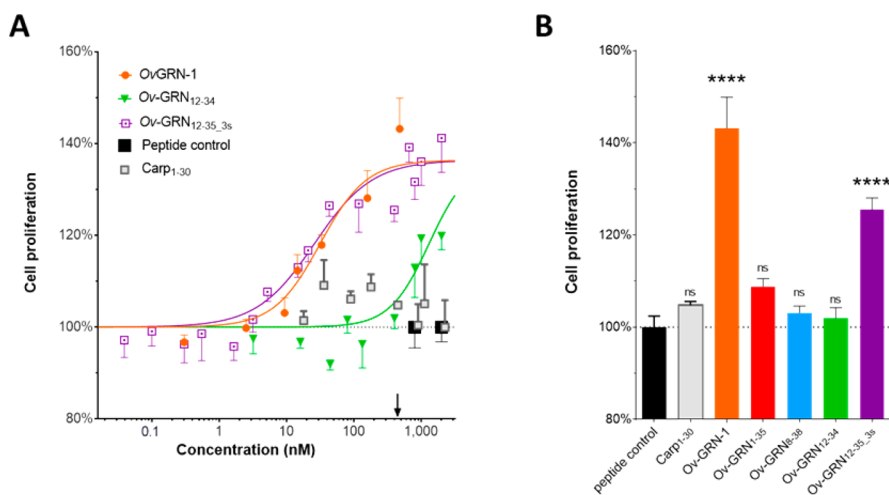


**Figure 4.** Liver fluke granulin peptides induce cell proliferation. (A) *Opisthorchis viverrini* granulin peptides but not carp granulin<sub>1–30</sub> induced proliferation of H69 human cholangiocytes at a range of concentrations as monitored using xCELLigence. Only selected treatments are graphed to aid visualization. Variable slope dose response lines of best fit show proliferation 4 days after a single application of treatment. *Ov*-GRN<sub>12–35\_3s</sub> potency characterized by significantly increased cell proliferation observed at final concentrations of  $\geq 15$  nM ( $p < 0.05$ ). Black arrow denotes 400–483 nM concentration used in (B). (B) Mean proliferation at 400 nM of all *Ov*-GRN-1 synthesized peptides and 483 nM *Ov*-GRN-1 protein from (A). ns = not significant, \*\*\*\* $p < 0.0001$ . Both panels: Two-Way ANOVA test with Dunnett's correction for multiple comparisons was used to compare treatments with relevant treatment controls (*Ov*-GRN-1 protein relative to thioredoxin expression matched recombinant protein control and peptides relative to peptide control (20-residue peptide derived from tropomyosin)). Mean values from four to six replicates pooled from two to four experiments with SEM bars shown either above or below for clarity.

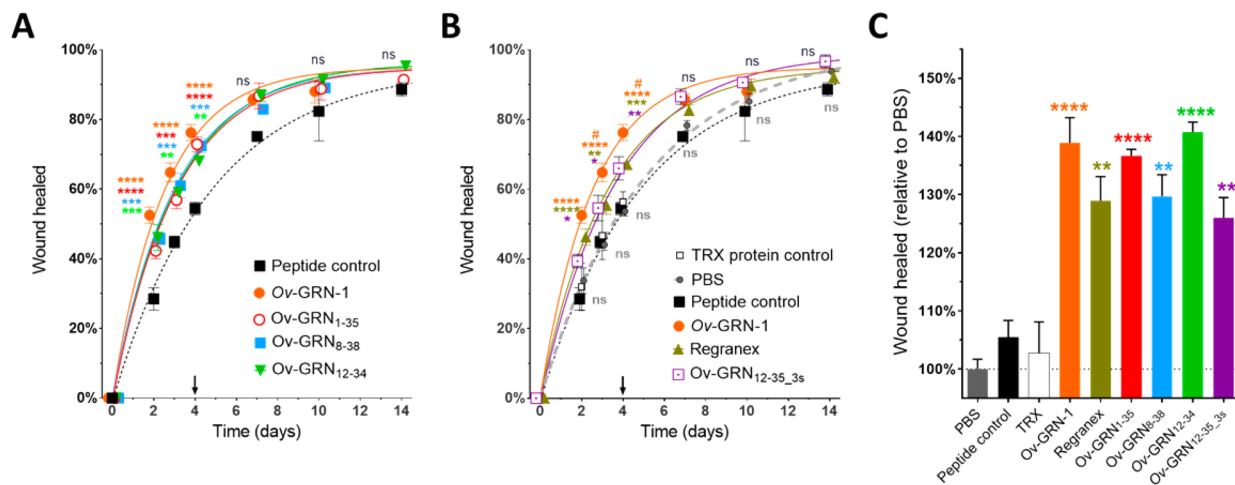


**Figure 5.** Mouse wound healing activity of *Ov*-GRN-1 and peptides. (A,B) Wound healing outcomes from treatments with 56 pmol of recombinant *Ov*-GRN-1, *Ov*-GRN-1 peptides, unrelated peptide, thioredoxin (TRX) protein controls, and 71 pmol Regranex in 1.5% methylcellulose gel applied daily in 50  $\mu$ L volume from days 0–4 to a  $\sim 0.2$  cm<sup>2</sup> wound arising from biopsy punch to the scalp between the ears. To aid visualization, data were split across two graphs with the *Ov*-GRN-1 and peptide control groups shown in both panels. No significant differences between the unrelated peptide control, PBS, or TRX protein control were noted at any time point. Black arrows denote the day 4 time point used in (C). (C) Wound healing relative to PBS vehicle control from day 4. All panels: mean healing rates of 2–6 biological replicates of groups of 4–5 animals plotted with SEM bars. Groups have been marginally shifted left or right to aid viewing. Repeated measure Two-Way ANOVA test with Dunnett's correction for multiple comparisons compare each group against each other group. Significance against peptide/protein control signified by \*\*\*\* =  $p < 0.0001$ , \*\*\* =  $p < 0.001$ , \*\* =  $p < 0.01$ , \* =  $p < 0.05$ , ns = not significant. Significant treatments against Regranex signified by # =  $p < 0.05$ . Color of asterisk or hash represents the relevant group. The colors and symbols are maintained across Figures 2–5.

understood, and uncertainty remains about potential receptors for this growth factor.<sup>19,20</sup>

*Ov*-GRN-1 appears to have distinct folding pathways compared to other granulins. The N-terminal region of *Ov*-GRN-1, comprising two native disulfide bonds (Cys I–Cys III and Cys II–Cys V), does not fold independently into a native-like  $\beta$ -hairpin structure, in contrast to carp granulin-1 and human granulin A. It is noteworthy that the introduction of a third, non-native disulfide bond in *Ov*-GRN<sub>12–35\_3s</sub> results in a

$\beta$ -hairpin structure similar to that present in the carp granulin-1 and human granulin A peptides.<sup>14,15</sup> The disulfide bond connectivity of *Ov*-GRN<sub>12–35\_3s</sub> appears to comprise the two native disulfide bonds (Cys I–Cys III and Cys II–Cys V) in addition to the Cys IV–Cys VI disulfide bond. If the bond pairs are conserved across species,<sup>7,9</sup> the latter bond is predicted not to be present in the full length *Ov*-GRN-1, as Cys IV is predicted to bond to Cys VII and Cys VI to Cys IX.

The paraganulin (half-granulin) domain of mammal progranulin contains the equivalent six cysteine residues present in *Ov*-GRN<sub>12–35\_3s</sub> and is biologically active,<sup>21</sup> which suggests that *Ov*-GRN<sub>12–35\_3s</sub> potentially contains the same disulfide connectivity. Carp granulin<sub>1–30</sub> peptide might accommodate this Cys I–Cys III, Cys II–Cys V, and Cys IV–Cys VI connectivity.<sup>14</sup> Although carp granulin<sub>1–30</sub> peptide contains only the two native disulfide bonds (Cys I–Cys III and Cys II–Cys V), analysis of the structure indicates that the side chains of the serine residues, which replace Cys IV and Cys VI, are in close proximity (Figure 3) and suggest that it is feasible for these cysteine residues to form a disulfide bond.

The disulfide connectivity in *Ov*-GRN<sub>12–35\_3s</sub> has implications for the structure of full-length *Ov*-GRN-1, which has not been experimentally determined because sufficient quantities of correctly folded recombinant material remain unavailable. Therefore, the disulfide connectivity of the native protein has not been shown to conform to the connectivity originally shown for carp granulin-1.<sup>7</sup> It is conceivable that the protein contains a disulfide domain comprising the first six cysteine residues (equivalent to that seen in *Ov*-GRN<sub>12–35\_3s</sub>) and a second domain containing the last six cysteine residues. Without the structure of the full-length protein and a comparison to the native protein secreted by the parasite, this remains speculation. However, previous reports revealed ambiguity in the disulfide connectivity of granulins.<sup>9,15</sup> The structures of human granulin A and F have well-defined N-terminal regions, but disordered C-terminal regions prevented characterization of all the disulfide bonds. Furthermore, chemical analysis of the disulfide connectivity of human granulin A was inconclusive.<sup>9</sup>

In addition to providing insight into the folding of *Ov*-GRN-1, the current study revealed that the N-terminal region contributes to the bioactivity and the  $\beta$ -hairpin of *Ov*-GRN<sub>12–35\_3s</sub> further enhanced cell proliferation activity. However, the  $\beta$ -hairpin structure is far from the complete story in regard to proliferative activity, as the carp granulin<sub>1–30</sub> peptide contains dual  $\beta$ -hairpins and, in contrast to the *Ov*-GRN-1 peptides, showed no substantial proliferation at the eight concentrations tested (10 nM to 2  $\mu$ M). A comparison of the sequences of carp granulin-1 with *Ov*-GRN-1 reveals that there are only two conserved noncysteine residues between Cys I and Cys VI. This lack of conservation in the loop sequences likely accounts for the differences in both folding and bioactivity.

Despite the lack of native structure, the two-disulfide bond containing *Ov*-GRN-1 peptides promoted cell proliferation at high concentrations (>800 nM) and stimulated significant healing of cutaneous wounds in mice. *Ov*-GRN<sub>12–35\_3s</sub> was the most potent peptide in the cell proliferation assay but was no more active in vivo than the other *Ov*-GRN-1 peptides. If the  $\beta$ -hairpin of *Ov*-GRN<sub>12–35\_3s</sub> is involved in wound healing in vivo, we did not observe a difference in mice. Cell proliferation activity may be cell line specific, or alternatively the concentrations tested in mouse wound repair were not optimal. In either case, the activity observed in mice may be of greater biological and therapeutic consequence than findings from the in vitro analysis. In the future, we envision exploring a range of cells from diverse organs and tissues and investigation of mice that exhibit deficits in wound healing in order to increase our understanding of the role of *Ov*-GRN-1 structure–activity relationships.

## CONCLUSION

To conclude, structural analysis with NMR spectroscopy suggested that *Ov*-GRN-1 exhibits unique folding properties compared with other granulins, presumably resulting from primary sequence differences. We have identified a bioactive region of *Ov*-GRN-1, which is likely to be less immunogenic and more readily produced than the full-length recombinant protein. Peptides and derivatives of liver fluke granulin that maintain the bioactivity represent a key advance toward identification of novel therapies for treatment of wounds.

## EXPERIMENTAL SECTION

**Peptide Synthesis and Purification.** Truncated granulin peptides were synthesized using manual solid-phase peptide synthesis using fluorenylmethyloxycarbonyl (Fmoc) chemistry. Peptides were assembled on 2-chlorotriethyl chloride resin (Aussep, Australia). Amino acids were activated using 2-(1*H*-benzotriazol-1-yl)-1,1,3,3-tetramethyluronium hexafluorophosphate (HBTU, Iris Germany) in peptide grade dimethylformamide (DMF, Aussep, Australia). Peptides were cleaved using a mixture of 95% TFA/2.5% TIPS/2.5% H<sub>2</sub>O. The TFA was removed by evaporation with nitrogen, and ice-cold diethyl ether was added to the residue. Ether was removed by filtration, and the peptide was dissolved in 40% acetonitrile/water mixture containing 0.1% trifluoroacetic acid (TFA) and subsequently freeze-dried. The resulting crude peptides were purified with reversed phase high performance liquid chromatography (RP-HPLC) on a C-18 preparative column (Phenomenex Jupiter 10  $\mu$ m C<sub>18</sub> 300 Å 250 mm  $\times$  21.2 mm). Gradients of 1%/min of 0%–80% solvent B (90% acetonitrile in 0.045% TFA in H<sub>2</sub>O) and solvent A (aqueous 0.045% TFA in H<sub>2</sub>O) were used, and the eluent was monitored at 215 and 280 nm. Peptides were oxidized by stirring a solution of the peptide in 100 mM ammonium bicarbonate (pH 8.2) containing 5 mM reduced glutathione and left overnight at room temperature and purified using RP-HPLC on a C-18 preparative column (Phenomenex Jupiter 10  $\mu$ m C<sub>18</sub> 300 Å, 250 mm  $\times$  21.2 mm). The purity of the peptides was assessed using analytical RP-HPLC and all peptides had  $\geq$ 95% purity.

To confirm the disulfide connectivity of the truncated peptides, *Ov*-GRN<sub>12–34</sub> was synthesized with selective protection of the cysteine residues. Cys1 and Cys14 were side chain protected with ACM groups and Cys8 and Cys23 with (Trt) protecting groups. Following cleavage and purification of the crude peptide, the disulfide bond between Cys8 and Cys23 was formed in 100 mM ammonium bicarbonate and the peptide was purified using the procedure described above. The S-ACM groups were subsequently removed by stirring 2 mg of peptide in 0.5 mL of TFA, 10  $\mu$ L anisole, and 25 mg of silver trifluoromethanesulfonate at 4 °C for 1.5 h. Cold ether (10 mL) was added to the mixture and the precipitate collected by centrifugation. The precipitate was washed twice with ether and oxidized, without further purification, overnight using a solution of 50% DMSO in 0.5 M HCl. The solution was diluted 15 times with water, and the fully folded peptide was purified by HPLC using 1% ACN gradient on a C-18 preparative column (Phenomenex Jupiter 10  $\mu$ m C<sub>18</sub> 300 Å, 250 mm  $\times$  21.2 mm).

**Autoinduction of Recombinant Protein Expression in *E. coli*.** *Ov-grn-1* pET41a or *Escherichia coli* thioredoxin (*trx*) cDNAs contained within the pET32a (Novagen) plasmid were transfected into BL21 *E. coli* cells (Life Technologies) and used to create recombinant proteins with autoinduction as described.<sup>4,22</sup> Briefly, ZYM-5052 culture media were supplemented with 100  $\mu$ M Fe(III)Cl<sub>3</sub> and 100  $\mu$ g/L kanamycin to produce recombinant protein (r*Ov*-GRN-1) or 50  $\mu$ g/L ampicillin to produce TRX. Then 200200 mL of inoculated media in a 1 L baffled Erlenmeyer flask was incubated overnight at 37 °C at 300 rpm rotation to induce expression with autoinduction.

**Recombinant Protein Purification.** Purification of r*Ov*-GRN-1 was achieved using an AKTA10 purification system at 4 °C (GE Healthcare).<sup>23</sup> The BL21 *E. coli* pellet was lysed with three freeze/thaw cycles followed by sonication on ice with a Q4000 unit (Qsonix). Then 20 g of the resulting insoluble pellet was solubilized in 400 mL

of urea-containing nickel binding buffer (8 M urea/300 mM NaCl/50 mM imidazole/50 mM sodium phosphate pH 8 [Sigma]) at 4 °C for 24 h with slow agitation. The 0.22  $\mu$ M filtered supernatant was passed over 2  $\times$  5 mL HisTrap IMAC nickel columns (GE Healthcare) and washed with increasing imidazole concentrations (two column volumes [CV] at 50 mM/5 CV at 100 mM) and eluted with 500 mM imidazole in binding buffer. The control TRX protein was expressed in the same fashion but under native conditions (without chaotropic agents) and purified with HisTrap IMAC Nickel columns.<sup>23</sup>

**Protein Refolding and Purification.** Refolding of urea-denatured rOv-GRN-1 was performed with 28 mL of G10 Sephadex (GE) resin on a XK16/20 column (GE) as described.<sup>23</sup> A 120 mL Superdex 30 XK16/60 column (GE) was used to fractionate 3 mL of refolded rOv-GRN-1 into 150 mM NaCl, 50 mM sodium phosphate, pH 6, at a flow rate of 1 mL/min. Fractions containing rOv-GRN-1 monomer eluting at a size equivalent of  $\sim$ 1 kDa (based on the fold of granulin proteins despite a denatured molecular size of 10.4 kDa) were pooled. Protein concentration was determined by a combination of microplate Bradford assay (Biorad) and absorbance at 280 nm.

**NMR Spectroscopy and Structure Determination.** Purified peptides were dissolved in 90% $H_2O$ /10%  $D_2O$  to provide a  $\sim$ 0.2 mM stock. Two-dimensional  $^1H$ - $^1H$  TOCSY,  $^1H$ - $^1H$  NOESY,  $^1H$ - $^1H$  DQF-COSY,  $^1H$ - $^{15}N$  HSQC, and  $^1H$ - $^{13}C$  HSQC spectra were acquired at 290 K using a 600 MHz AVANCE III NMR spectrometer (Bruker, Karlsruhe, Germany) equipped with a cryogenically cooled probe. Spectra were recorded with an interscan delay of 1 s. NOESY spectra were acquired with a mixing time of 200 ms, and TOCSY spectra were acquired with an isotropic mixing period of 80 ms. All spectra were assigned using CCPNMR<sup>24</sup> based on the approach described by Wuthrich.<sup>25</sup> The  $\alpha$ H secondary shifts were determined by subtracting the random coil  $^1H$  NMR chemical shifts of Wishart<sup>26</sup> from experimental  $\alpha$ H chemical shifts.

The three-dimensional structures of Ov-GRN<sub>12-34</sub> and Ov-GRN<sub>12-35\_3s</sub> were determined. The 2D NOESY spectra were automatically assigned, and an ensemble of structures calculated using the program CYANA.<sup>27</sup> Torsion-angle restraints predicted using TALOS+ were used in the structure calculations. Disulfide-bond connectivities (Cys1-Cys14, Cys8-Cys23) were included in the calculations for Ov-GRN<sub>12-34</sub> because these bonds were confirmed by selective protection of the cysteine residues. Selective protection of the cysteine residues was not used for Ov-GRN<sub>12-35\_3s</sub> in an attempt to isolate the most energetically favorable form. Consequently, the structures were calculated with the 15 possible disulfide connectivities. An analysis of the CYANA target functions was carried out to determine the most likely connectivity. Structures were visualized using MOLMOL.<sup>28</sup>

**Mammalian Cell Culture.** The nonmalignant cholangiocyte cell line H69 is a SV40-transformed human bile duct epithelial cell line derived from human liver, kindly provided by Dr. Gregory J. Gores, Mayo Clinic, Rochester, Minnesota. H69 cells<sup>23,29,30</sup> were maintained in T75 cm<sup>2</sup> vented flasks (Corning) as monolayers as described<sup>31</sup> with minor modifications. Cells were maintained with regular splitting using 0.25% trypsin (Life Technologies) every 2–5 days in complete media [RPMI (Sigma)] with growth factor-supplemented specialist complete media<sup>30</sup> [DMEM/F12 with high glucose, 10% FCS, 1 $\times$  antibiotic/antimycotic, 25  $\mu$ g/mL adenine, 5  $\mu$ g/mL insulin, 1  $\mu$ g/mL epinephrine, 8.3  $\mu$ g/mL holo-transferrin, 0.62  $\mu$ g/mL hydrocortisone, 13.6 ng/mL T3, and 10 ng/mL EGF; Life Technologies]. Low nutrient media for cell proliferation assays was 5% complete media, i.e., 0.5% FCS and  $1/20$  of the growth factor concentrations listed above for complete media. The identities (human-derived) of the cell line were confirmed with single tandem repeat (STR) analysis in January 2015 (15/15 positive loci across two alleles) and mycoplasma free at the DNA Diagnostics Centre (DDC)–Medical (U.S.A.), accredited/certified by CAP, ISO/IEC 17025:2005, through ACLASS.

**Cell Proliferation Monitoring in Real Time Using xCELLigence.** Cells were seeded at 1500 cells/well in 180  $\mu$ L of complete media (above) in E-plates (ACEA Biosciences) and grown overnight while being monitored with an xCELLigence SP system (ACEA Biosciences), which monitors cellular events in real time by measuring

electrical impedance across interdigitated gold microelectrodes integrated into the base of tissue culture plates.<sup>32</sup> Cells were washed three times with PBS prior to addition of 180  $\mu$ L of low nutrient media (above) and incubated for a minimum of 6 h before further treatment. Treatments were prepared at 10 $\times$  concentration and added to each well in a total volume of 20  $\mu$ L. The xCELLigence system recorded cell indexes at intervals of 1 h for 5–6 days following treatment. Readings for the cell index were normalized prior to treatment, and cell proliferation ratios represent the relative numbers of cells compared to control cells at day 4. Dose response curves for each peptide were generated from 3 to 6 independent experiments each with 4–6 replicates. Comparisons of induction of cell proliferation in response to treatments were accomplished using Two-Way ANOVA test with Dunnett's multiple comparison correction, using GraphPad Prism 6.02.

**Mouse Wounding Assay.** These studies were conducted with the approval of the James Cook University Small Animal Ethics Committee, applications A1806 and A2204, as described.<sup>6</sup> Briefly, female 11–12 week old BALB/c mice weighing 19–23 g were sourced from the Australian ARC (Animal Resources Centre) and randomly allocated into groups of 4–5 mice. Mice were anesthetized (intraperitoneal xylazine 16 mg/kg; ketamine 80 mg/kg), after which a skin-deep wound on the crown of the head was inflicted using a 5 mm biopsy punch (Zivic instruments). Betadine liquid antiseptic (Sanofi) was applied, followed by application of 50  $\mu$ L that contained either 71 pmol of Regranex (treatment of 71 pmol equals 1  $\mu$ g per 0.25 cm<sup>2</sup> wound, as recommended by manufacturer Smith and Nephew), 56 pmol of rOv-GRN-1, Ov-GRN-1 peptides, control peptide (EADRYDEVARKLAMVEADL), TRX, or PBS suspended in 1.5% methylcellulose (Sigma). Wounds were photographed daily, and after blinding treatment, groups the area of the lesion was measured with ImageJ software and plotted as percent of wound closure from original wound images. Wound healing rates were compared with Two-Way ANOVA test with Dunnett's correction for multiple comparisons, using GraphPad prism 6.02. Each mouse wounding study was conducted at least twice to provide reproducibility.

## ■ ASSOCIATED CONTENT

### 📄 Supporting Information

The Supporting Information is available free of charge on the ACS Publications website at DOI: 10.1021/acs.jmedchem.7b00047.

Structure statistics for Ov-GRN<sub>12-34</sub> and Ov-GRN<sub>12-35\_3s</sub>; chemical shift analysis of carp granulin-1; analysis of different disulfide connectivities for Ov-GRN<sub>12-35\_3s</sub>; wound healing photos (PDF)

Ov-GRN<sub>12-34</sub> (PDB)

Ov-GRN<sub>12-35</sub> (PDB)

PDB 1QGM (PDB)

### Accession Codes

The PDB ID codes are 5UJH and 5UJG for Ov-GRN<sub>12-34</sub> and Ov-GRN<sub>12-35\_3s</sub>, respectively. Authors will release the atomic coordinates and experimental data upon article publication.

## ■ AUTHOR INFORMATION

### Corresponding Authors

\*For N.L.D.: phone, +61-7-4232 1815; E-mail, [norelle.daly@jcu.edu.au](mailto:norelle.daly@jcu.edu.au).

\*For A.L.: phone, +61-7-4232 1608; E-mail, [alex.loukas@jcu.edu.au](mailto:alex.loukas@jcu.edu.au).

### ORCID

Norelle L. Daly: 0000-0002-4697-6602

### Author Contributions

§P.S.B. and M.J.S. contributed equally to this research.

## Notes

The authors declare no competing financial interest.

## ACKNOWLEDGMENTS

This research was supported by an R01 grant from the National Cancer Institute, USA (R01CA164719), and a program grant from National Health and Medical Research Council, Australia (NHMRC) (1037304). Fellowship support was provided to A.L. from NHMRC (1020114) and N.L.D. from the Australian Research Council (FF110100226). The content is solely the responsibility of the authors and does not necessarily represent the official views of the NCI or NIH. The funders had no role in study design, data collection and analysis, decision to publish, or preparation of the manuscript.

## ABBREVIATIONS USED

Fmoc, fluorenylmethyloxycarbonyl; Ov-GRN, *Opisthorchis viverrini* granulin; PBS, phosphate buffered saline; PGRN, progranulin; TRX, thioredoxin

## REFERENCES

- (1) He, Z.; Ong, C. H.; Halper, J.; Bateman, A. Progranulin is a mediator of the wound response. *Nat. Med.* **2003**, *9*, 225–229.
- (2) Mulvenna, J.; Sripa, B.; Brindley, P. J.; Gorman, J.; Jones, M. K.; Colgrave, M. L.; Jones, A.; Nawaratna, S.; Laha, T.; Suttiprapa, S.; Smout, M. J.; Loukas, A. The secreted and surface proteomes of the adult stage of the carcinogenic human liver fluke *Opisthorchis viverrini*. *Proteomics* **2010**, *10*, 1063–1078.
- (3) Laha, T.; Pinlaor, P.; Mulvenna, J.; Sripa, B.; Sripa, M.; Smout, M. J.; Gasser, R. B.; Brindley, P. J.; Loukas, A. Gene discovery for the carcinogenic human liver fluke. *BMC Genomics* **2007**, *8*, 189.
- (4) Smout, M. J.; Laha, T.; Mulvenna, J.; Sripa, B.; Suttiprapa, S.; Jones, A.; Brindley, P. J.; Loukas, A. A granulin-like growth factor secreted by the carcinogenic liver fluke, *Opisthorchis viverrini*, promotes proliferation of host cells. *PLoS Pathog.* **2009**, *5*, e1000611.
- (5) Smout, M. J.; Sripa, B.; Laha, T.; Mulvenna, J.; Gasser, R. B.; Young, N. D.; Bethony, J. M.; Brindley, P. J.; Loukas, A. Infection with the carcinogenic human liver fluke. *Mol. BioSyst.* **2011**, *7*, 1367–1375.
- (6) Smout, M. J.; Sotillo, J.; Laha, T.; Papatpremsiri, A.; Rinaldi, G.; Pimenta, R. N.; Chan, L. Y.; Johnson, M. S.; Turnbull, L.; Whitchurch, C. B.; Giacomini, P. R.; Moran, C. S.; Golledge, J.; Daly, N.; Sripa, B.; Mulvenna, J. P.; Brindley, P. J.; Loukas, A. Carcinogenic parasite secretes growth factor that accelerates wound healing and potentially promotes neoplasia. *PLoS Pathog.* **2015**, *11*, e1005209.
- (7) Hrabal, R.; Chen, Z.; James, S.; Bennett, H. P.; Ni, F. The hairpin stack fold, a novel protein architecture for a new family of protein growth factors. *Nat. Struct. Biol.* **1996**, *3*, 747–752.
- (8) Ong, C. H.; Bateman, A. Progranulin (granulin-epithelin precursor, PC-cell derived growth factor, acrogranin) in proliferation and tumorigenesis. *Histol. Histopathol.* **2003**, *18*, 1275–1288.
- (9) Tolkatchev, D.; Malik, S.; Vinogradova, A.; Wang, P.; Chen, Z.; Xu, P.; Bennett, H. P.; Bateman, A.; Ni, F. Structure dissection of human progranulin identifies well-folded granulin/epithelin modules with unique functional activities. *Protein Sci.* **2008**, *17*, 711–724.
- (10) Alquezar, C.; de la Encarnacion, A.; Moreno, F.; Lopez de Munain, A.; Martin-Requero, A. Progranulin deficiency induces overactivation of WNT5A expression via TNF- $\alpha$ /NF- $\kappa$ B pathway in peripheral cells from frontotemporal dementia-linked granulin mutation carriers. *J. Psychiatry Neurosci.* **2016**, *41*, 225–239.
- (11) Park, B.; Buti, L.; Lee, S.; Matsuwaki, T.; Spooner, E.; Brinkmann, M. M.; Nishihara, M.; Ploegh, H. L. Granulin is a soluble cofactor for toll-like receptor 9 signaling. *Immunity* **2011**, *34*, 505–513.
- (12) Yeh, J. E.; Kreimer, S.; Walker, S. R.; Emori, M. M.; Krystal, H.; Richardson, A.; Ivanov, A. R.; Frank, D. A. Granulin, a novel STAT3-interacting protein, enhances STAT3 transcriptional function and correlates with poorer prognosis in breast cancer. *Genes Cancer.* **2015**, *6*, 153–168.
- (13) Yip, C. W.; Cheung, P. F.; Leung, I. C.; Wong, N. C.; Cheng, C. K.; Fan, S. T.; Cheung, S. T. Granulin-epithelin precursor interacts with heparan sulfate on liver cancer cells. *Carcinogenesis* **2014**, *35*, 2485–2494.
- (14) Vranken, W. F.; Chen, Z. G.; Xu, P.; James, S.; Bennett, H. P.; Ni, F. A 30-residue fragment of the carp granulin-1 protein folds into a stack of two beta-hairpins similar to that found in the native protein. *J. Pept. Res.* **1999**, *53*, 590–597.
- (15) Tolkatchev, D.; Ng, A.; Vranken, W.; Ni, F. Design and solution structure of a well-folded stack of two beta-hairpins based on the amino-terminal fragment of human granulin A. *Biochemistry* **2000**, *39*, 2878–2886.
- (16) Wishart, D. S.; Bigam, C. G.; Holm, A.; Hodges, R. S.; Sykes, B. D.  $^1\text{H}$ ,  $^{13}\text{C}$  and  $^{15}\text{N}$  random coil NMR chemical shifts of the common amino acids. I. Investigations of nearest-neighbor effects. *J. Biomol. NMR* **1995**, *5*, 67–81.
- (17) Saether, O.; Craik, D. J.; Campbell, I. D.; Sletten, K.; Juul, J.; Norman, D. G. Elucidation of the primary and three-dimensional structure of the uterotonic polypeptide kalata B1. *Biochemistry* **1995**, *34*, 4147–4158.
- (18) Daly, N. L.; Koltay, A.; Gustafson, K. R.; Boyd, M. R.; Casafinet, J. R.; Craik, D. J. Solution structure by NMR of circulin A: a macrocyclic knotted peptide having anti-HIV activity. *J. Mol. Biol.* **1999**, *285*, 333–345.
- (19) Chen, X.; Chang, J.; Deng, Q.; Xu, J.; Nguyen, T. A.; Martens, L. H.; Cenik, B.; Taylor, G.; Hudson, K. F.; Chung, J.; Yu, K.; Yu, P.; Herz, J.; Farese, R. V., Jr.; Kukar, T.; Tansey, M. G. Progranulin does not bind tumor necrosis factor (TNF) receptors and is not a direct regulator of TNF-dependent signaling or bioactivity in immune or neuronal cells. *J. Neurosci.* **2013**, *33*, 9202–9213.
- (20) Etemadi, N.; Webb, A.; Bankovacki, A.; Silke, J.; Nachbur, U. Progranulin does not inhibit TNF and lymphotoxin- $\alpha$  signalling through TNF receptor 1. *Immunol. Cell Biol.* **2013**, *91*, 661–664.
- (21) Rollinson, S.; Young, K.; Bennion-Callister, J.; Pickering-Brown, S. M. Identification of biological pathways regulated by PGRN and GRN peptide treatments using transcriptome analysis. *Eur. J. Neurosci.* **2016**, *44*, 2214–2225.
- (22) Studier, F. W. Protein production by auto-induction in high density shaking cultures. *Protein Expression Purif.* **2005**, *41*, 207–234.
- (23) Smout, M. J.; Mulvenna, J. P.; Jones, M. K.; Loukas, A. Expression, refolding and purification of Ov-GRN-1, a granulin-like growth factor from the carcinogenic liver fluke, that causes proliferation of mammalian host cells. *Protein Expression Purif.* **2011**, *79*, 263–270.
- (24) Vranken, W. F.; Boucher, W.; Stevens, T. J.; Fogh, R. H.; Pajon, A.; Llinas, M.; Ulrich, E. L.; Markley, J. L.; Ionides, J.; Laue, E. D. The CCPN data model for NMR spectroscopy: development of a software pipeline. *Proteins: Struct., Funct., Genet.* **2005**, *59*, 687–696.
- (25) Wüthrich, K. *NMR of Proteins and Nucleic Acids*; Wiley-Interscience: New York, 1986.
- (26) Wishart, D. S.; Bigam, C. G.; Yao, J.; Abildgaard, F.; Dyson, H. J.; Oldfield, E.; Markley, J. L.; Sykes, B. D.  $^1\text{H}$ ,  $^{13}\text{C}$  and  $^{15}\text{N}$  chemical shift referencing in biomolecular NMR. *J. Biomol. NMR* **1995**, *6*, 135–140.
- (27) Guntert, P. Automated NMR structure calculation with CYANA. *Methods Mol. Biol.* **2004**, *278*, 353–378.
- (28) Koradi, R.; Billeter, M.; Wüthrich, K. MOLMOL: a program for display and analysis of macromolecular structures. *J. Mol. Graphics* **1996**, *14*, 29–32.
- (29) Grubman, S. A.; Perrone, R. D.; Lee, D. W.; Murray, S. L.; Rogers, L. C.; Wolkoff, L. I.; Mulberg, A. E.; Cherington, V.; Jefferson, D. M. Regulation of intracellular pH by immortalized human intrahepatic biliary epithelial cell lines. *Am. J. Physiol.: Gastroenterol. Liver Physiol.* **1994**, *266*, G1060–G1070.
- (30) Matsumura, T.; Takesue, M.; Westerman, K. A.; Okitsu, T.; Sakaguchi, M.; Fukazawa, T.; Totsugawa, T.; Noguchi, H.; Yamamoto, S.; Stolz, D. B.; Tanaka, N.; Leboulch, P.; Kobayashi, N. Establishment of an immortalized human-liver endothelial cell line with SV40T and hTERT. *Transplantation* **2004**, *77*, 1357–1365.

(31) Papatpremsiri, A.; Smout, M. J.; Loukas, A.; Brindley, P. J.; Sripa, B.; Laha, T. Suppression of *Ov-grn-1* encoding granulin of *Opisthorchis viverrini* inhibits proliferation of biliary epithelial cells. *Exp. Parasitol.* **2015**, *148*, 17–23.

(32) Xing, J. Z.; Zhu, L.; Jackson, J. A.; Gabos, S.; Sun, X. J.; Wang, X. B.; Xu, X. Dynamic monitoring of cytotoxicity on microelectronic sensors. *Chem. Res. Toxicol.* **2005**, *18*, 154–161.